HHS Public Access

Author manuscript

Mol Imaging Biol. Author manuscript; available in PMC 2024 June 20.

Published in final edited form as:

Mol Imaging Biol. 2024 February ; 26(1): 124–137. doi:10.1007/s11307-023-01840-7.

2nd Window NIR Imaging of Radiation Injury Mitigation Provided by Reduced Notch-Dll4 Expression on Vasculature

Mir Hadi Razeghi Kondelaji[1], **Guru Prasad Sharma**[2], **Jaidip Jagtap**[3], **Shayan Shafiee**[1], **Christopher Hansen**[1], **Tracy Gasperetti**[2], **Anne Frei**[2], **Dana Veley**[2], **Jayashree Narayanan**[2], **Brian L. Fish**[2], **Abdul K. Parchur**[2], **El-Sayed H. Ibrahim**[4], **Meetha Medhora**[2], **Heather A. Himburg**[2], **Amit Joshi**[1]

[1]Department of Biomedical Engineering, Medical College of Wisconsin, Milwaukee, WI, USA

[2]Department of Radiation Oncology, Medical College of Wisconsin, Milwaukee, WI, USA

[3]Department of Radiology, Mayo Clinic, Rochester, MN, USA

[4]Department of Radiology, Medical College of Wisconsin, Milwaukee, WI, USA

Abstract

Purpose—Vascular endothelium plays a central role in the pathogenesis of acute and chronic radiation injuries, yet the mechanisms which promote sustained endothelial dysfunction and contribute to late responding organ failure are unclear. We employed 2nd window (> 1100 nm emission) Near-Infrared (NIR) imaging using indocyanine green (ICG) to track and define the role of the notch ligand Delta-like ligand 4 (Dll4) in mediating vascular injury in two late-responding radiosensitive organs: the lung and kidney.

Procedures—Consomic strains of female Salt Sensitive or SS (Dll4-high) and SS with 3rd chromosome inherited from Brown Norway, SS.BN3 (Dll4-low) rats at ages 11–12 weeks were used to demonstrate the impact of reduced Dll4 expression on long-term vascular integrity, renal function, and survival following high-dose 13 Gy partial body irradiation at 42- and 90 days post-radiation. 2nd window dynamic NIR fluorescence imaging with ICG was analyzed with physiology-based pharmacokinetic modeling and confirmed with assays of endothelial Dll4 expression to assess the role of endogenous Dll4 expression on radiation injury protection.

Results—We show that SS.BN3 (Dll4-low) rats are relatively protected from vascular permeability disruption compared to the SS (Dll4-high) strain. We further demonstrated that SS.BN3 (Dll4-low) rats have reduced radiation induced loss of $CD31^+$ vascular endothelial cells, and increased Dll4 vascular expression is correlated with vascular dysfunction.

Conclusions—Together, these data suggest Dll4 plays a key role in pathogenesis of radiation-induced vascular injury to the lung and kidney.

✉Heather A. Himburg, hhimburg@mcw.edu, Amit Joshi, ajoshi@mcw.edu.
Mir Hadi Razeghi Kondelaji and Guru Prasad Sharma contributed equally to the manuscript.

Competing Interests The authors declare no competing interests.

Supplementary Information The online version contains supplementary material available at https://doi.org/10.1007/s11307-023-01840-7.

Keywords

Near-infrared (NIR) fluorescence imaging; Indocyanine green (ICG); Delta-like ligand 4 (Dll4); Consomic rat model; Vascular permeability; NIR-1 window; NIR-2 window

Introduction

Following radiation exposure, the vascular endothelium of acutely radiosensitive organs such as the bone marrow and gastrointestinal tract undergoes well-defined pathophysiological changes including inflammation[1, 2], cell death [3, 4], altered gene expression [5, 6], and decreased barrier function [6]. Importantly, rescue of normal endothelial integrity and function has been positively associated with survival in the acute syndromes of hematopoietic and gastrointestinal radiation injury [1, 7, 9] that occur in the first month after radiation. However, survivors of high-dose acute radiation exposure have an elevated lifetime risk of developing a range of late multi-organ morbidities which are collectively referred to as the delayed effects of acute radiation exposure (DEARE). While DEARE encompasses a broad range of inflammatory and fibrotic morbidities, sustained vascular dysfunction is common to multiple radiation-sensitive tissues including the lung [10, 11], kidneys, heart [12–15], and brain [16]. Late vascular dysfunction is characterized by structural changes in the vasculature including malformities [16], and vessel regression [10, 17]. Previously, we demonstrated increased pulmonary vascular permeability in response to radiation injury with near-infrared-1 window (~ 800 nm) optical imaging and validated the imaging based vascular permeability assay with multiple gold standard techniques including measurement of pulmonary vascular filtration coefficient, Evan's blue dye-based permeability assay, and lung histology [18].

Here, we define the potential role of Delta-like ligand 4 (Dll4) in mediating the observed radiation-induced long-term alterations in vascular structure and function. Dll4 is an endothelial-specific Notch ligand which is necessary for normal vascular development. There are no direct reports showing the reduction in radiation-induced endothelial dysfunction following Dll4 reduction in the context of the delayed effects of the radiation injury. In murine tumor models, Dll4 blockade has been shown to inhibit tumor growth and angiogenesis [19]. Recently, using cervical cancer cell line models, it was shown that Dll-4 inhibition radiosensitizes these cells via the inhibition of cell proliferation, promotion of radiation-induced apoptosis, and inhibition of DNA damage repair. Loss of even one Dll4 allele results in defective vascular development and embryonic lethality in most mouse strains [20–22]; therefore, we have leveraged a previously established consomic rat model of reduced Dll4 expression [23]. In this consomic rat model, the third chromosome in the female salt-sensitive or Dahl-SS rat is substituted with chromosome 3 from the Brown Norway rat with lower Dll4 expression [23, 24]. Prior work in this model demonstrated dysfunctional tumor angiogenesis in the SS.BN3 (Dll4-low) strain relative to the SS (Dll4-high) strain. Since there are multiple gene candidates on BN 3rd chromosomes, these vascular phenotypes were also validated in congenic and sub-congenic strains by introgressions of varying segments of BN chromosome 3 into the parental SS strain to localize the role of SS Dll4 on tumor angiogenesis with precision [23, 24]. SS.BN3

(Dll4-low) rats have reduced radiation-induced cardiotoxicity relative to SS (Dll4-high) rats [25]. Here, we evaluate the susceptibility of SS.BN3 (Dll4-low) rats to progressive radiation-induced vascular dysfunction and compare the response of the SS.BN3 (Dll4-low) to the SS (Dll4-high) strain to radiation injury using an established DEARE model [26, 27].

To non-invasively track changes in vascular permeability in the lung and kidney, we used a second window Near-Infrared (NIR) imaging approach with the FDA-cleared dye, Indocyanine Green (ICG), which significantly decreases tissue background autofluorescence and is less impacted by multiple scattering [28, 29]. Multiple investigators have demonstrated that the signal to noise ratio greatly improves with fluorescent emission at 900 nm–1500 nm (NIR-2 window) compared to the ~ 800 nm (NIR-1 window) [30]. NIR-1 cyanine fluorophores like ICG have off- peak tail emission that exceeds 1000 nm and can provide excellent NIR-2 imaging capability [29]. Compared to NIR-1 window imaging with ICG, the ICG NIR-2 window imaging provides clearer vascular structure in mice [31]. While 2nd window NIR imaging has been demonstrated in ~ 20 g mouse models for tumor imaging [32], it has not been reported for sensitive organ level vascular function imaging in large ~ 200 g rats. To image the changes in vascular biology pertinent to radiation injury, we demonstrate that 2nd window NIR imaging allows reproducible, sensitive, and robust discrimination of vascular injury and recovery in Dll4-low vs Dll4-high rat strains. The contrast agent kinetics from surface-weighted NIR imaging was verified with high temporal resolution ultrashort echo (UTE) based dynamic contrast-enhanced MRI of *in vivo* lung cross-sections with gadolinium contrast agent (Gadovist™). Using the combination of novel NIR imaging, image-based pharmacokinetic modeling, a unique rat strain with reduced Dll4 expression, and our established DEARE model, we can demonstrate the critical role Dll4 in mediating long-term vascular dysfunction and survival following radiation injury.

Methods

Approved protocols by Medical College of Wisconsin Institutional Biosafety Committee (IBC) and Institutional Animal Care and Use Committee (IACUC, OLAW-NIH Animal Welfare Assurance D16-00064(A3102-01)) were followed for all reported studies and ARRIVE guidelines were followed [33]. SS, SS.BN3, and Wag/RijCmcr rats were used for *in vivo* and *ex vivo* assays for studying the impact of radiation on pulmonary and renal endothelial cells (ECs), the role of Dll4 and target notch pathway genes via transcriptional, and/or flow cytometry studies of protein expression. The study design and the strain and number of rats used in each experiment have been illustrated in Table 1.

Animals and Partial Body Irradiation (PBI) Model

Dahl-SS.BN3 which inherit the 3rd chromosome from Brown Norway (BN) rats were developed as part of the Consomic Xenograft Model at the Medical College of Wisconsin (MCW)[34] (Fig. 1a). Dahl-SS, Dahl-SS.BN3, and WAG/RijCmcr were purchased from the Rat Research Models Service Center at the Medical College of Wisconsin. All animal studies were performed on isoflurane anesthetized animals. For survival analysis in response to radiation injury, adult 11–12-week-old Dahl-SS (n = 13) or Dahl-SS.BN3 (n = 19) female rats were exposed to 13 Gy partial body irradiation (PBI) with 8% bone marrow shielding

to one hind-limb (Pantak, 300 kVp; 169 cGy/min, 1.4 mm Cu HVL)[35]. All rats received supportive care post-radiation consisting of antibiotics (enrofloxacin ~ 10 mg/kg/day) in the drinking water from days 2–14, subcutaneous saline (40 mL/kg) days 3–7, and powdered diet days 35–70. Additionally, body weight, respiration, and renal function were monitored to assess the health of the rats. Rats were followed for survival through gastrointestinal, hematopoietic, lung and renal injury up to 160 days. Details for blood urea nitrogen (BUN) and cardiac output (heart rate and stroke volume) determination are provided in supplementary data.

1st and 2nd Window "*In Vivo*" NIR Fluorescence Imaging

The imaging setup comprised of 785 nm (Thorlabs) or 808 nm (Diomed, D15 Plus) diode lasers for illumination and an image intensified cooled CCD for NIR-1 imaging (PIMAX-4 512EMB, Princeton Instruments Inc., Trenton, NJ, USA) or an InGaAs focal plane array for NIR-2 imaging (NIRvana 640ST, Princeton Instruments Inc., Trenton, NJ, USA). For both NIR-1 and NIR-2 imaging, holographic notch filters to reject excitation light (785 nm: SuperNotch-Plus™, HSPF-785.0–2.0, Kaiser Optical System, Ann Arbor, MI,808 nm: NF03-808E-50, Semrock, StopLine®) were employed. NIR-1 emission was captured with 830 nm bandpass filter (830FS10-25, Andover, Salem, NH) with 785 nm excitation (0.6 mW/cm^2), NIR-2 emission was captured with 950 nm (Semrock, EdgeBasic™, BLP01-980R-50) or 1100 nm (FELH1100, Thorlabs) long pass filters positioned following the holographic notch rejections filters in the optical path(the 808 nm holographic notch was not used in conjunction with the 1100 nm long pass). Dynamic contrast-enhanced NIR-2 fluorescence imaging was performed on anesthetized rats for 15 min following ICG injection with a temporal resolution of 50 ms [18]. ICG dose was about 1 mg/kg delivered by tail vein injection with a syringe pump at 0.2 mg/s. The lungs were imaged at: 42 days post-radiation (total of 32 SS and 35 SS.BN3 rats, i.e., SS 0 Gy (n = 17), SS 13 Gy (n = 15), SS.BN3 0 Gy (n = 13), and SS.BN3 13 Gy (n = 22)) and 90 days post-radiation (total of 22 SS and 29 SS.BN3 rats, i.e., SS 0 Gy (n = 9), SS 13 Gy (n = 13), SS.BN3 0 Gy (n = 12), and SS.BN3 13 Gy (n = 17)). The kidneys were imaged at day 90 (total of 16 SS and 19 SS.BN3 rats, i.e., SS 0 Gy (n = 11), SS 13 Gy (n = 15), SS.BN3 0 Gy (n = 7), and SS.BN3 13 Gy (n = 12)).

NIR Image Processing

Images were processed in MATLAB (R2021b MATHWORKS Inc.). The image frames were assembled as 3-D arrays (2-space and 1-time dimension) for all animals. Raw imaging data was acquired over 25–30 min post injection for all animals. The intensity time series data for each pixel was truncated to first 16,384 frames and corrected with a Fourier band pass filter to denoise and remove respiratory motion artifacts (Supplementary Video SV1 a and b)[18]. Finally, for consistency between all animals and computational efficacy, data was further truncated to 8192 frames or 12.88 min of imaging time post injection. Principal component analysis (PCA) along the time-dimension was used to convert the imaging data to a k-component vector for each pixel, where k is the number of time-frames in the original dataset. The first 8-components were used to identify organ ROIs[18]. The PCA components which clearly identified the lungs or kidneys were selected, and their decomposed matrix (images) were used to define the region of interest (ROI) for either the lungs (Supplementary

Fig. S3) or kidneys (Supplementary Fig. S4). The average intensity time-series of segmented ROI was calculated and normalized via the intensity at 28 s post ICG injection, and the normalized intensity-time course was plotted for all experimental groups and compared via statistical tests.

Physiology-Based Pharmacokinetic Modeling (PBPK) of NIR Fluorescence-Derived ICG Uptake and Clearance

Recently, we developed a PBPK model to describe the pulmonary uptake and clearance of ICG[18]. This 2-compartment model which includes cardiac output describes the ICG exchange and retention between and within vascular and tissue compartments to estimate parameters that significantly affect the ICG uptake and clearance by the lungs, including the permeability of the pulmonary vascular endothelium (Fig. 3e). The exchange rate of ICG concentration in each compartment is given by the following ordinary differential equation (ODE) system:

$$V_b\frac{dC_b}{dt} = F((1-\alpha)C_{in} - C_b) + PS(C_t - C_b) \tag{1}$$

$$V_t\frac{dC_t}{dt} = PS(C_b - C_t) + V_t(k_{-1}C_e - (k_1 + k_2)C_t) \tag{2}$$

$$V_t\frac{dC_e}{dt} = V_t(k_1C_t - k_{-1}C_e) \tag{3}$$

$$V_t\frac{dC_d}{dt} = V_t(k_2C_t) \tag{4}$$

$$V_b\frac{dC_B}{dt} = F(\alpha C_{in} - C_B) \tag{5}$$

$$\frac{dC_{in}}{dt} = \left(\frac{d_0}{BV}\right) \times S_P - \left(\frac{C_{in}}{\tau}\right), \quad for \;\; t > T_{inj}, S_P = 0 \tag{6}$$

where $C_b = C_t = C_e = C_d = C_B = 0$ μM at $t = 0$ and d_0 is injected dose of ICG and is based on rat weight. C_{in} is the concentration of ICG in blood supply to lungs. F

(mL/min) is the rat cardiac output, α is the fraction of injected dye that is plasma protein or albumin bound, C_B (μM) is the plasma protein-bound ICG concentration in the vasculature, C_e (μM) is the ICG concentration in the lung tissue, C_d (μM) is the ICG concentration of irreversibly bound dye in the tissue, and V_b (mL) and V_t (mL) are the vascular region and apparent tissue volume respectively. Four important parameters can be calculated from Eqs. 1–6, including PS (mL/min) which is the lung vascular permeability-surface area product and describes the diffusion of ICG between vascular and tissue compartments. K_1 and K_{-1} $\left(\min^{-1}\right)$ are the forward and backward rate constants of the dye reversible binding within the tissue region, and K_2 $\left(\min^{-1}\right)$ is forward rate constant of the dye tightly bound within tissue region. $S_p = 0.2$ ml/sec is the pump speed, and BV is the blood volume. Blood volume is estimated based on rat weight according to the established formula: BV [mL] = 0.06 × body weight (g) + 0.77 (mL)[18, 36]. The cardiac output (F) and the ICG half-life (τ) were independently calculated (Supplementary Table 1, Supplementary Table 2, and Supplementary Fig. 2).

In Vitro Endothelial Cell Radiation Study

Rat Primary Lung Microvascular Endothelial Cells were purchased from Cell Biologics (cat no. RA-6011) and cultured in Rat Endothelial Cell Medium Supplement Kit (Cell Biologics, cat. no. M1266) as recommended by the manufacturer in a 5% CO_2 and 95% air in a humidified incubator. At 70–80% confluency, ECs were radiated with an 8 Gy dose and harvested at defined time points for transcriptional analysis. Cells with passages 2–3 were used in the experiment. Transcriptional analysis of Dll4, and target notch genes was done at 6 h, 24 h, and 72 h post-radiation.

Flow Cytometry Analysis of Endothelial Cell and Dll4 Expression Changes

Single endothelial cell suspension from tissue was prepared as previously described [37]. About ten million lung cells per animal were used for $CD31^+$ enrichment using the CD31 Microbeads kit (cat# 130–109–680, Miltenyi) as per the manufacturer's instructions.

Flow cytometry assays was adapted from our previous study [38]. Briefly, one million lung cells were surface stained with fluorophore-labelled monoclonal antibodies: PE-CD31 (FAB3628P, R&D systems) and APC-CD45 (17–0461–82, Thermo Fisher). Dll4 cell surface staining was done using unconjugated rabbit anti-rat primary antibody (NB600-892, R&D systems) followed by staining with secondary Pacific Blue Goat Anti-Rabbit IgG (P-10994, Thermo Fisher). The antibody staining was done at 4 °C for 30 min in staining buffer (1XPBS with 2% FBS). Single color tubes were used to set up a compensation matrix and a Fluorescence Minus One (FMO) control was included to ensure specific staining. 7-AAD (420,404, Bio Legend) was used to exclude dead cells. The data were acquired on a MACSQuant 10 Analyzer Flow Cytometer (Miltenyi) and analyzed using FlowJo software version 10.0 (BD Life Sciences). To verify gating and purity, all populations were routinely backgated.

Quantitative Transcriptional Studies with RT-qPCR

Total RNA was isolated from lung tissue using RNeasy Micro Kit (cat no. 74004, Qiagen) following the manufacturer's instructions and reverse transcribed to cDNA using the High-Capacity RNA-to-cDNA™ Kit (cat no. 4387406, Thermo Fisher Scientific). Quantitative real-time PCR was performed using the TaqMan Gene Expression Assay primer probes (cat no. 4331182, Thermo Fisher Scientific). The rat primer probes used were Dll4 (Rn01512886) and the reference GAPDH (Rn01775763). Expression of target genes was normalized to GAPDH. The relative expression of the gene was calculated with respect to control (0 Gy) and presented as fold change ($2^{-(\Delta Ct\ subject)-(mean\ \Delta Ct\ control)}$), statistics done on ΔCt values.

Statistical Analysis

While the data corresponding to non-irradiated control groups was normally distributed, imaging and terminal assay results from the radiated groups were often non-normally distributed; thus, a robust method was chosen to test for significance, and strategies such as log-normalization were not employed. For all the reported parameters and direct measurements, linear model regression was performed via customized scripts in the statistical language "R" with radiation dose and rat strain as covariates. The linear regression output was analyzed with 2-way ANOVA to generate the *P* values which indicated whether the groups significantly differed with respect to radiation dose or strain. Pairwise post hoc comparison with the Sidak test was performed to identify which specific group pairs differed significantly (****$P < 0.0001$, ***$P < 0.001$, **$P < 0.01$, and *$P < 0.05$).

Results

SS.BN3 (Dll4-Low) Rats Have Improved Median Survival Following Radiation Injury

As previously described[24], SS.BN3 (Dll4-low) rats were generated by the substitution of chromosome 3 from the Brown Norway rat into the Dahl-SS rat (Fig. 1a). Dll4 expression was previously shown to be reduced in the tumor vasculature of SS.BN3 rats relative to SS rats[24] Here, we validated the decreased expression of Dll4 mRNA in the lung vasculature of SS.BN3 rats relative to SS rats (Fig. 1b). At baseline, lung endothelial mRNA expression of Dll4 was twofold reduced in SS.BN3 rats relative to SS rats ($P = 0.0061$). We then evaluated whether there were differences in susceptibility to morbidity due to lung and kidney DEARE between the SS.BN3 (Dll4-low) and SS (Dll4-high) rats. Rats were exposed to 13 Gy PBI and were followed day 160 for signs of morbidity due to lung or renal failure. Kaplan–Meier survival curves are plotted in Fig. 1c. Median survival in the SS.BN3 (Dll4-low) rats was increased from 129 days in the SS (Dll4-high) rats to 155 days, while all nonirradiated rats survived to 155 days. The *P* value for the log-rank comparison was $P = 0.0002$. Change in body weight for this same cohort of irradiated rats is shown over time in Fig. 1d. A typical precursor of morbidity in this radiation model is a drop in body weight which is indicative of declining general health. Consistent with the improvement in median survival, SS.BN3 rats (Dll4-low) rats tended to have less body weight loss overall and had significantly reduced body weight loss at day 90 (during radiation pneumonitis) and day 120 following radiations (coinciding with the onset of radiation nephropathy) than SS (Dll4-high) rats (Fig. 1d).

Radiation Induces Increase in Vascular Permeability in SS (Dll4-High) Rats but Not SS.BN3 (Dll4-Low) Rats

We assessed the differences in lung and kidney vascular permeability between SS.BN3 rats (Dll4-low) and SS (Dll4-high) rats at day 42 and at day 90 post irradiation using non-invasive 2 nd window NIR imaging (Fig. 2a). These time-points were chosen on the basis of prior studies which identified the time intervals for lung injury via pneumonitis at 40–70 days and recovery at 70–90 days, with renal injury detectable at 90 days and reaching morbid levels by 110 days[39]. Representative raw videos are included as supplemental data (Supplementary Video SV2 a–d) and (Supplementary Video SV3 a–d). The three imaging setups were compared for lung and kidney visualization in anesthetized healthy rats. Principle component analysis (PCA) was used to define the region of interest (ROI) for either the right lung and right kidney imaging (Fig. 2b), and the best components with high fidelity to anatomical organs were selected for comparison of NIR-1 and NIR-2 ICG imaging techniques (PIMAX—830 nm, NIRVANA—950 nm, and NIRVANA—1100 nm emission) (Supplementary Fig. 3 and 4). As shown in Fig. 2b, PCA outcome quality successively improved with emission windows from NIR-1 (830 nm bandpass) to 950 nm long pass and decomposed images of 1100 nm + NIR-2 window represented best defined contours for both kidneys and lungs. Also, both organs were more prominently visualized with longer wavelength long pass filters (NIRVANA—1100 nm) compared to shorter wavelength bandpass or long pass filters (PIMAX—830 nm; NIRVANA—950 nm); thus, the NIR-2 setting with 1100 long pass emission was chosen for all successive experiments (see Supplementary Video SV4 a–d). Figure 3a, b depicts the kinetics of ICG fluorescence diffusion in the right lung for each group at day 42 (Fig. 3a) and day 90 (Fig. 3b). In general, radiation increased the residence time of the ICG in tissue indicating vascular leakage due to an increase in vessel permeability at both 42- and 90-day time-points; however, the effect was far larger at day 42, and a recovery was observed at day 90. We implemented a mixed-effects covariance model for 8192 timesteps with time-varying covariates, to analyze the average fluorescence intensity of ICG in the right lung where subject numbers serve as the repeated measure indicator and the rat strain serving as covariate. The model was used to locate time steps with the most covariance parameter significance as an indicator of radiation effect. The covariance parameters represent significant effect of radiation injury at 42 days post-radiation, but it decreases at 90 days (Fig. 3c) indicating recovery in surviving animals. The diagonal projection of covariance on a time axis (Fig. 3d) suggests a significant covariance parameter in late timesteps, suggesting radiation effect on delayed clearance of ICG and hence changes in lung vascular permeability. Similar contrast agent uptake and clearance profiles were observed with cross-sectional UTE MRI with Gadovist™ (Supplementary Fig. 1) thus confirming trends observed with optical imaging. For the lungs, the kinetic data were fit to the previously described physiology-based pharmacokinetic model (PBPK) to calculate a quantitative estimate of the vascular permeability surface area (PS) At day 42 or around peak pulmonary vascular injury timeframe, PS in SS (Dll4-high) rats exposed to 13 Gy increased threefold (PS value is 6.85 [CI: 4.30–9.41] for irradiated SS (Dll4-high) rats) compared to nonradiated SS (Dll4-high) control rats (PS value is 2.36 [CI: 2.1–2.62] for non-radiated SS (Dll4-high) rats) (Fig. 3f). Conversely, no significant difference in permeability at day 42 was observed in SS.BN3 (Dll4-low) rats exposed to radiation (Fig. 3f). The fraction of ICG bound to all plasma proteins (α) was not significantly

different between all 4 groups which was 0.91 [CI: 0.89–0.93] and 0.86 [CI: 0.81–0.92] for control and irradiated SS rats, respectively. The fraction was 0.87 [CI: 0.84–0.90] and 0.89 [CI: 0.88–0.90] for control and irradiated SSBN3 rats. No significant differences in PS value in either SS or SS.BN3 control and radiated groups were observed at day 90, at which point the surviving rats had overcome lung vascular injury (Fig. 3f). Thus, the imaging derived PS parameter could adequately explain the survival differences in SS (Dll4-high) and SS.BN3 (Dll4-low) rats. Similar to 42 time points, there was no significant difference for the parameter α between 4 groups at 90-day time point where it was 0.87 [CI: 0.83–0.91] for control SS rats, 0.89 [CI: 0.87–0.90] for irradiated SS rats, 0.91 [CI: 0.90–0.92] for control SSBN3 rats, and 0.92 [CI: 0.91–0.92] for irradiated SSBN3 rats.

SS.BN3 (Dll4-Low) Rats Have Reduced Radiation-Induced Loss of CD31 + Endothelial Cells

We next examined radiation-induced changes in endothelial cellularity in lung and kidney at day 70 post-irradiation. At baseline, SS.BN3 (Dll4-low) rats have a significantly lower percentage of $CD31^+$ endothelial cells compared to SS (Dll4-high) rats in both the lungs and kidneys (Fig. 4a, b). While the number of C $D31^+$ endothelial cells is lower in SS.BN3 (Dll4-low) at baseline, SS.BN3 rats do not exhibit a loss of endothelial cells following radiation in these tissues at day 70 after PBI. Conversely, following 13 Gy radiation injury, the frequency of endothelial cells in both the lung and kidneys of SS (Dll4-high) rats is significantly reduced compared to 0 Gy (Fig. 4a, b) while the frequency of lung and kidney endothelial cells in SS.BN3 (Dll4-low) rats is unchanged by radiation (Fig. 4a, b), and this data can verify the *in vivo* imaging results reported in Fig. 3.

SS.BN3 (Dll4-Low) Are Less Sensitive to Radiation-Induced Renal Vascular Damage

Next, we examined the progression to renal failure in SS.BN3 (Dll4-low) and SS (Dll4-high) rats. At the 13 Gy partial body irradiation dose used in this model, all rats eventually succumb to morbidity due to progressive renal failure. Optical imaging for progressive renal injury was performed at 90 days. Observed trends in ICG wash-in and washout were identical to lung imaging, indicating a similar nature of endothelial cell response to radiation in the kidneys as well. SS (Dll4-high) rat kidney ICG kinetics was significantly affected by radiation, whereas the contrast agent kinetics in SS.BN3 (Dll4-low) rats were not different post 13 Gy radiation. The imaging kinetics of the right kidney at day 90 are shown in Fig. 5a. Renal function was monitored by measuring blood urea nitrogen (BUN) levels, an endogenous marker of renal function. BUN levels were significantly higher in SS (Dll4-high) rats (n = 30 for 90 days and n = 8 for 120 days) at both days 90 and 120 post-radiation compared to SS.BN3 (Dll4-low) (n = 37 for 90 days and n = 24 for 120 days) (Fig. 5b). Consistent with the reduced BUN values in SS.BN3 (Dll4-low) rats, we observed improved retention of glomerular endothelial cells in SS.BN3 (Dll4-low) rats versus SS (Dll4-high) rats (Fig. 5c and Supplementary Fig. 5). Representative images of glomeruli stained with the rat endothelial-specific antibody RECA-1 (Fig. 5c) illustrate the higher number of RECA-1 + (brown) endothelial cells in the glomeruli of SS.BN3 (Dll4-low) rats relative to SS (Dll4-high) rats (n = 4 per group). The percentage of endothelial cells per glomeruli was quantified (as described by Cowley et al.)[40] and is illustrated in Fig. 5c and Supplementary Fig. 5. While the percentage of glomerular endothelial cells was significantly

reduced in SS (Dll4-high) rats, glomerular endothelial cells were not significantly changed in SS.BN3 (Dll4-low) rats (Fig. 5d) following radiation.

Radiation Regulates Endothelial Dll4 Expression

In the acute setting, radiation has previously been shown to increase endothelial Notch signaling [41, 42]. Consistent with these prior reports, we observed 8 Gy *ex vivo* irradiation of pulmonary endothelial cells increased transcription of Notch target genes Hes1 and Hey2 at 6, 24, and 72 h following irradiation (Fig. 6a). We then assessed late radiation-induced changes in endothelial Dll4 transcription and protein expression at day 70 post-irradiation *in vivo*. In the lung endothelium, Dll4 transcription was reduced in both SS (Dll4-high) rats and SS.BN3 (Dll4-low) rats; however, this reduction was significant in SS (Dll4-high) rats (Fig. 6b). We confirmed this response in a third rat strain, the WAG/RijCmcr at days 28, 42, and 70 following 13.5 Gy PBI (Fig. 6c). Dll4 transcription was significantly downregulated in the lung endothelium of the WAG/RijCmcr rat at days 42 and 70 post-PBI compared to age-matched non-irradiated control rats (Fig. 6c). Expression of Notch target genes Hey2 and Hes1 had a non-significant increase at 28 post-PBI but was decreased by day 70 post-PBI relative to 0 Gy control rats (Fig. 6c). However, when we examined cell surface expression of Dll4 on ECs by FACS, we observed that the fraction of $Dll4^+$ ECs increased in both the lung and kidney of irradiated SS (Dll4-high) rats (Fig. 6d). Conversely, the fraction of $Dll4^+$ endothelial cells was unchanged in SS.BN3 (Dll4-low) rats (Fig. 6d). Similar to the SS (Dll4-high) rat, cell surface levels of Dll4 were also significantly increased in the lung endothelium of the WAG/RijCmcr rat at days 42 and 70 following 13.5 Gy PBI (Fig. 6e).

Discussion

2^{nd} window NIR dynamic contrast imaging not only allowed the clear, live visualization of the lungs and kidneys in 200 g rats for ROI-based image analysis but also enabled the image-based pharmacokinetic analysis of vascular function in these organs. According to the prior studies, ICG tightly binds to plasma proteins including plasma albumin, high-density lipoprotein (HDL), and low-density lipoprotein (LDL) which reduces the amount of free ICG in the blood plasma and limits the exchange of ICG with tissue region[43]. This binding property has been modeled in our PBPK equations by a dimensionless parameter α that is the fraction of plasma protein-bound ICG and can take any number between 0 and 1. Our modeling indicate the high fraction of protein-bound ICG in the blood plasma (around 0.9) for all groups, including control and irradiated groups, suggesting that a significant fraction of ICG is protein bound and may not penetrate the smaller capillaries; however, there is no radiation effect on the fraction of protein- bound ICG in the blood plasma. The model-fitted permeability-surface area product PS accurately reflected the increased pulmonary vascular injury in Dll4-high SS rats at 42 days with recovery to normal range at 90 days in surviving animals. Further, the kinetic profile of reduced washout rate following radiation injury in SS-rats (Fig. 3a) corresponded to reduced Dll4 expression following radiation (Fig. 4). For Dll4-low SS.BN3 rats, both the imaging PBPK model derived PS values and the measured Dll4 expression on endothelial cells did not alter upon radiation injury. Similar to lungs, increased retention of ICG was observed in the kidney imaging for the SS rats (Fig. 5a) which can be attributed to disruption of ICG bound protein filtering by the glomerulus.

Glomerulus endothelium injury precedes the damage to tubules [44]. While a water solution dye such as IRDye800 can investigate kidney function comprehensively, ICG with its albumin binding can provide an early indication of glomerulus injury and protein leakage. While ICG retention has been used previously for measuring the renal vascular perfusion for surgery applications[45, 46], here, we show that ICG imaging can indicate enhanced glomerulus disruption in the Dll4-high SS rat strain in response to radiation injury. This is the first-time, quantitative, and reproducible ICG 2nd window fluorescence imaging has been reported in animal models 10 times the size of mice for assessing vascular injury in interior organs. Similar to NIR-1 imaging, NIR-2 imaging with Indocyanine green fluorescence will be limited to 2–3-cm tissue depths, which can provide whole body organ level imaging in mice and rat models of radiation injury, but human use will be limited to either tissue depths of 3 cm from skin surface, or by using endoscopic or bronchoscopy imaging methods.

In this study, we have identified the notch ligand Dll4 as a driver of lung and kidney endothelial dysfunction following radiation injury. Consomic SS.BN3 rats with lower Dll4 expression had markedly improved survival compared to SS (Dll4-high) rats, especially in the first 120 days following radiation. Importantly, SS.BN3 (Dll4-low) rats were protected against vascular injury as evidenced by maintenance of vascular permeability and protection of endothelial cell numbers. We believe the decreased endothelial expression of Dll4 likely plays a role in this observed radioprotection based on our correlative findings which showed SS.BN3 (Dll4-low) rats have reduced baseline transcription of Dll4 compared to SS rats. This is verified by the fluorescence imaging of ICG uptake and clearance, where SS.BN3 (Dll4-low) rats indicate slower ICG clearance compared to SS (Dll4-high) even at baseline in absence of radiation injury. Additionally, while the fraction of Dll4-expressing endothelial cells increases in the SS (Dll4-high) rats, we see no radiation-induced differences in Dll4^{+} endothelial cells in the SS.BN3 (Dll4-low) rats. Although the findings described here may not be entirely attributable to loss of Dll4 as multiple genes are known to be differentially expressed between endothelial cells derived from these consomic strains[24], these findings are consistent with prior observations that Dll4 has gene dosage/expression dependent effects on blood vessel regulation[22, 47, 48]. Our observations in the SS.BN3 (Dll4-low) rat strain are consistent with this notion as we observe a twofold reduction in Dll4 expression improves vascular recovery.

In the acute response to radiation injury, endothelial Notch signaling plays an essential role in the regeneration of the bone marrow microenvironment as endothelial-specific deletion of either Notch ligands Jagged-1 or Jagged-2 prevents hematopoietic stem cell reconstitution following myelosuppressive radiation injury[49–51]. However, sustained upregulation of Notch signaling post-radiation may promote pathological vessel remodeling in non-hematopoietic tissues as aberrant Notch signaling is associated with vascular dysfunction in other diseases[52]. In the gene expression analyses performed here, we do see an immediate increase in Notch signaling as indicated by upregulation of the Notch target genes hes1 and hey2. However, at time point later than 42 days following *in vivo* radiation exposure, both Dll4 and Notch target genes are downregulated in the lung endothelium. Curiously, despite the transcriptional downregulation of Dll4, we do see an increase in the fraction of Dll4-expressing endothelial cells. This finding may suggest endothelial Dll4 expression confers relative radio-resistance as has been previously observed in some cancer

cell lines [53]. Our observation that Dll4-low rats are protected against radiation-induced morbidities suggests Dll4 may be a therapeutic target for suppressing pathological vascular remodeling following radiation injury. In conclusion, we have observed dynamic regulation of Dll4-Notch signaling in response to radiation and injury which was imageable with 2nd windo3w NIR fluorescence imaging. To further elucidate the mechanisms which initiate long-term endothelial dysfunction after radiation, future studies will examine acute changes in the lung vascular endothelium at the single cell level.

Supplementary Material

Refer to Web version on PubMed Central for supplementary material.

Funding

This work was supported by funding from NIH/NIAID U01AI133594 (PI H. Himburg), U01AI138331 (PI M. Medhora), NIH/NCI 2R01CA193343 (PI A. Joshi), MCW Department of Radiation Oncology, and the MCW Cancer Center.

Data Availability

This study employed the established consomic rat models SS and SS.BN3. The publicly accessible and NIH supported Rat Genome Database (rgd.mcw.edu) catalogs and has tools to explore the genotype and phenotype information for the SS (Dll4-high) and SS.BN3 (Dll4-low) strains under strain records RRID: RGD_61499 and RRID: RGD_1358154, respectively. The PBPK analysis codes are available by request from the corresponding author.

References

1. Kim A, Seong KM, Choi YY, Shim S, Park S, Lee SS (2020) Inhibition of EphA2 by dasatinib suppresses radiation-induced intestinal injury. Int J Mol Sci 21(23):9096. 10.3390/ijms21239096 [PubMed: 33265912]
2. Wang J, Boerma M, Fu Q, Hauer-Jensen M (2007) Significance of endothelial dysfunction in the pathogenesis of early and delayed radiation enteropathy. World J Gastroenterol 13(22):3047–3055 [PubMed: 17589919]
3. Li XM, Hu Z, Jorgenson ML, Wingard JR, Slayton WB (2008) Bone marrow sinusoidal endothelial cells undergo nonapoptotic cell death and are replaced by proliferating sinusoidal cells in situ to maintain the vascular niche following lethal irradiation. Exp Hematol 36(9):1143–1156 [PubMed: 18718416]
4. Wang Y, Boerma M, Zhou D (2016) Ionizing radiation-induced endothelial cell senescence and cardiovascular diseases. Radiat Res 186(2):153–161 [PubMed: 27387862]
5. Cary L, Noutai D, Salber R, Fadiyimu O, Gross A, Almeida-Porada G, Kidane Y, Whitnall M (2019) Bone marrow endothelial cells influence function and phenotype of hematopoietic stem and progenitor cells after mixed neutron/gamma radiation. Int J Mol Sci 20(7):1795. 10.3390/ijms20071795 [PubMed: 30978983]
6. Chen Q, Liu Y, Jeong HW, Stehling M, Dinh VV, Zhou B, Adams RH (2019) Apelin(+) endothelial niche cells control hematopoiesis and mediate vascular regeneration after myeloablative injury. Cell Stem Cell 25(6):768–783 e766 [PubMed: 31761723]
7. Jang H, Lee J, Park S, Kim JS, Shim S, Lee SB, Han SH, Myung H, Kim H, Jang WS et al. (2019) Baicalein mitigates radiation-induced enteritis by improving endothelial dysfunction. Front Pharmacol 10:892 [PubMed: 31474856]

8. Li B, Bailey AS, Jiang S, Liu B, Goldman DC, Fleming WH (2010) Endothelial cells mediate the regeneration of hematopoietic stem cells. Stem Cell Res 4(1):17–24 [PubMed: 19720572]
9. Rotolo JA, Fong CS, Bodo S, Nagesh PK, Fuller J, Sharma T, Piersigilli A, Zhang Z, Fuks Z, Singh VK et al. (2021) Anticeramide single-chain variable fragment mitigates radiation GI syndrome mortality independent of DNA repair. JCI Insight 6(8):e145380. 10.1172/jci.insight.145380 [PubMed: 33724956]
10. Ghosh SN, Wu Q, Mader M, Fish BL, Moulder JE, Jacobs ER, Medhora M, Molthen RC (2009) Vascular injury after whole thoracic x-ray irradiation in the rat. Int J Radiat Oncol 74(1):192–199
11. Robbins ME, Brunso-Bechtold JK, Peiffer AM, Tsien CI, Bailey JE, Marks LB (2012) Imaging radiation-induced normal tissue injury. Radiat Res 177(4):449–466 [PubMed: 22348250]
12. Unthank JL, Miller SJ, Quickery AK, Ferguson EL, Wang M, Sampson CH, Chua HL, DiStasi MR, Feng H, Fisher A (2015) Delayed effects of acute radiation exposure in a murine model of the h-ars: multiple-organ injury consequent to< 10 gy total body irradiation. Health Phys 109(5):511 [PubMed: 26425910]
13. Unthank JL, Ortiz M, Trivedi H, Pelus LM, Sampson CH, Sellamuthu R, Fisher A, Chua HL, Plett A, Orschell CM et al. (2019) Cardiac and renal delayed effects of acute radiation exposure: organ differences in vasculopathy, inflammation, senescence and oxidative balance. Radiat Res 191(5):383–397 [PubMed: 30901530]
14. Boerma M, Hauer-Jensen M (2010) Potential targets for intervention in radiation-induced heart disease. Curr Drug Targets 11(11):1405–1412 [PubMed: 20583977]
15. Baker JE, Fish BL, Su J, Haworth ST, Strande JL, Komorowski RA, Migrino RQ, Doppalapudi A, Harmann L, Allen Li X et al. (2009) 10 gy total body irradiation increases risk of coronary sclerosis, degeneration of heart structure and function in a rat model. Int J Radiat Biol 85(12):1089–1100 [PubMed: 19995235]
16. Andrews RN, Bloomer EG, Olson JD, Hanbury DB, Dugan GO, Whitlow CT, Cline JM (2020) Non-human primates receiving high-dose total-body irradiation are at risk of developing cerebrovascular injury years postirradiation. Radiat Res 194(3):277–287 [PubMed: 32942304]
17. Mehrvar S, Mostaghimi S, Camara AK, Foomani F, Narayanan J, Fish B, Medhora M, Ranji M (2021) Three-dimensional vascular and metabolic imaging using inverted autofluorescence. J Biomed Opt 26(7):076002. 10.1117/1.jbo.26.7.076002 [PubMed: 34240589]
18. Jagtap J, Audi S, Razeghi-Kondelaji MH, Fish BL, Hansen C, Narayan J, Gao F, Sharma G, Parchur AK, Banerjee A et al. (2021) A rapid dynamic *in vivo* near-infrared fluorescence imaging assay to track lung vascular permeability after acute radiation injury. Am J Physiol Lung Cell Mol Physiol 320(3):L436–L450 [PubMed: 33404364]
19. Noguera-Troise I, Daly C, Papadopoulos NJ, Coetzee S, Boland P, Gale NW, Lin HC, Yancopoulos GD, Thurston GJN (2006) Blockade of dll4 inhibits tumour growth by promoting non-productive angiogenesis. Nature 444(7122):1032–1037 [PubMed: 17183313]
20. Gale NW, Dominguez MG, Noguera I, Pan L, Hughes V, Valenzuela DM, Murphy AJ, Adams NC, Lin HC, Holash J et al. (2004) Haploinsufficiency of delta-like 4 ligand results in embryonic lethality due to major defects in arterial and vascular development. Proc Natl Acad Sci U S A 101(45):15949–15954 [PubMed: 15520367]
21. Krebs LT, Shutter JR, Tanigaki K, Honjo T, Stark KL, Gridley T (2004) Haploinsufficient lethality and formation of arteriovenous malformations in notch pathway mutants. Genes Dev 18(20):2469–2473 [PubMed: 15466160]
22. Duarte A, Hirashima M, Benedito R, Trindade A, Diniz P, Bekman E, Costa L, Henrique D, Rossant J (2004) Dosage-sensitive requirement for mouse dll4 in artery development. Genes Dev 18(20):2474–2478 [PubMed: 15466159]
23. Sharma G, Jagtap JM, Parchur AK, Gogineni VR, Ran S, Bergom C, White SB, Flister MJ, Joshi A (2020) Heritable modifiers of the tumor microenvironment influence nanoparticle uptake, distribution and response to photothermal therapy. Theranostics 10(12):5368–5383 [PubMed: 32373218]
24. Flister MJ, Tsaih SW, Stoddard A, Plasterer C, Jagtap J, Parchur AK, Sharma G, Prisco AR, Lemke A, Murphy D et al. (2017) Host genetic modifiers of nonproductive angiogenesis inhibit breast cancer. Breast Cancer Res Treat 165(1):53–64 [PubMed: 28567545]

25. Schlaak RA, Frei A, Schottstaedt AM, Tsaih S-W, Fish BL, Harmann L, Liu Q, Gasperetti T, Medhora M, North PE et al. (2019) Mapping genetic modifiers of radiation-induced cardiotoxicity to rat chromosome 3. Am J Physiol Heart Circul Physiol 316(6):H1267–H1280
26. Fish BL, MacVittie TJ, Szabo A, Moulder JE, Medhora M (2020) Wag/rijcmcr rat models for injuries to multiple organs by single high dose ionizing radiation: Similarities to nonhuman primates (nhp). Int J Radiat Biol 96(1):81–92 [PubMed: 30575429]
27. Medhora M, Gao F, Gasperetti T, Narayanan J, Khan AH, Jacobs ER, Fish BL (2019) Delayed effects of acute radiation exposure (deare) in juvenile and old rats: Mitigation by lisinopril. Health Phys 116(4):529–545 [PubMed: 30624354]
28. Wang T, Chen Y, Wang B, Gao X, Wu M (2022) Recent progress in second near-infrared (nir-ii) fluorescence imaging in cancer. Biomolecules 12(8):1044 [PubMed: 36008937]
29. Zhu S, Hu Z, Tian R, Yung BC, Yang Q, Zhao S, Kiesewetter DO, Niu G, Sun H, Antaris AL et al. (2018) Repurposing cyanine nir-i dyes accelerates clinical translation of near-infrared-ii (nir-ii) bioimaging. Advanced Materials 30(34):1802546
30. Smith AM, Mancini MC, Nie S (2009) Bioimaging: second window for in vivo imaging. Nat Nanotechnol 4(11):710–711 [PubMed: 19898521]
31. Starosolski Z, Bhavane R, Ghaghada KB, Vasudevan SA, Kaay A, Annapragada A (2017) Indocyanine green fluorescence in second near-infrared (nir-ii) window. PLoS ONE 12(11):e0187563 [PubMed: 29121078]
32. Chi C, Ye J, Ding H, He D, Huang W, Zhang G-J, Tian J (2013) Use of indocyanine green for detecting the sentinel lymph node in breast cancer patients: from preclinical evaluation to clinical validation. PLoS ONE 8(12):e83927 [PubMed: 24358319]
33. Kilkenny C, Browne WJ, Cuthill IC, Emerson M, Altman DG (2010) Improving bioscience research reporting: the arrive guidelines for reporting animal research. PLoS Biol 8(6):e1000412 [PubMed: 20613859]
34. Flister MJ, Endres BT, Rudemiller N, Sarkis AB, Santarriaga S, Roy I, Lemke A, Geurts AM, Moreno C, Ran S et al. (2014) Cxm: a new tool for mapping breast cancer risk in the tumor microenvironment. Can Res 74(22):6419–6429
35. Fish BL, MacVittie TJ, Gao F, Narayanan J, Gasperetti T, Scholler D, Sheinin Y, Himburg HA, Hart B, Medhora M (2021) Rat models of partial-body irradiation with bone marrow-sparing (leg-out pbi) designed for fda approval of countermeasures for mitigation of acute and delayed injuries by radiation. Health Phys 121(4):419–433 [PubMed: 34546222]
36. Lee HB, Blaufox MD (1985) Blood volume in the rat. J Nuclear Med: Official Publication, Soc Nuclear Med 26(1):72–76
37. Sharma GP, Fish BL, Frei AC, Narayanan J, Gasperetti T, Scholler D, Pierce L, Szalewski N, Blue N, Medhora M, Himburg HA (2022) Pharmacological ACE-inhibition mitigates radiation-induced pneumonitis by suppressing ACE-expressing lung myeloid cells. Int J Radiat Oncol Biol Phys 113(1):177–191. 10.1016/j.ijrobp.2022.01.023 [PubMed: 35093482]
38. Sharma GP, Frei AC, Narayanan J, Gasperetti T, Veley D, Amjad A, Albano K, Fish BL, Himburg HA (2021) Brain-derived neurotrophic factor promotes immune reconstitution following radiation injury via activation of bone marrow mesenchymal stem cells. PLoS ONE 16(10):e0259042 [PubMed: 34695155]
39. Fish BL, Gao F, Narayanan J, Bergom C, Jacobs ER, Cohen EP, Moulder JE, Orschell CM, Medhora M (2016) Combined hydration and antibiotics with lisinopril to mitigate acute and delayed high-dose radiation injuries to multiple organs. Health Phys 111(5):410–419 [PubMed: 27682899]
40. Bukowy JD, Dayton A, Cloutier D, Manis AD, Staruschenko A, Lombard JH, Solberg Woods LC, Beard DA, Cowley AW Jr (2018) Region-based convolutional neural nets for localization of glomeruli in trichrome-stained whole kidney sections. J Am Soc Nephrol 29(8):2081–2088 [PubMed: 29921718]
41. Banerjee D, Barton SM, Grabham PW, Rumeld AL, Okochi S, Street C, Kadenhe-Chiweshe A, Boboila S, Yamashiro DJ, Connolly EP (2020) High-dose radiation increases notch1 in tumor vasculature. Int J Radiat Oncol Biol Phys 106(4):857–866 [PubMed: 31759078]

42. Scharpfenecker M, Kruse JJ, Sprong D, Russell NS, Ten Dijke P, Stewart FA (2009) Ionizing radiation shifts the pai-1/id-1 balance and activates notch signaling in endothelial cells. Int J Radiat Oncol Biol Phys 73(2):506–513 [PubMed: 19147015]
43. Yoneya S, Saito T, Komatsu Y, Koyama I, Takahashi K, Duvoll-Young J (1998) Binding properties of indocyanine green in human blood. Invest Ophthalmol Vis Sci 39(7):1286–1290 [PubMed: 9620093]
44. Baradaran-Ghahfarokhi M (2012) Radiation-induced kidney injury. J Renal Inj Prev 1(2):49–50 [PubMed: 25340106]
45. Arichi N, Mitsui Y, Ogawa K, Nagami T, Nakamura S, Hiraoka T, Yasumoto H, Shiina H (2014) Intraoperative fluorescence vascular imaging using indocyanine green for assessment of transplanted kidney perfusion. Transpl Proc 46(2):342–345
46. Mitsui Y, Shiina H, Arichi N, Hiraoka T, Inoue S, Sumura M, Honda S, Yasumoto H, Igawa M (2012) Indocyanine green (icg)based fluorescence navigation system for discrimination of kidney cancer from normal parenchyma: Application during partial nephrectomy. Int Urol Nephrol 44(3):753–759 [PubMed: 22215306]
47. Trindade A, Djokovic D, Gigante J, Badenes M, Pedrosa AR, Fernandes AC, Lopes-da-Costa L, Krasnoperov V, Liu R, Gill PS et al. (2012) Low-dosage inhibition of dll4 signaling promotes wound healing by inducing functional neo-angiogenesis. PLoS ONE 7(1):e29863 [PubMed: 22279550]
48. Djokovic D, Trindade A, Gigante J, Pinho M, Harris AL, Duarte A (2015) Incomplete dll4/notch signaling inhibition promotes functional angiogenesis supporting the growth of skin papillomas. BMC Cancer 15:608 [PubMed: 26314892]
49. Poulos MG, Ramalingam P, Gutkin MC, Kleppe M, Ginsberg M, Crowley MJP, Elemento O, Levine RL, Rafii S, Kitajewski J et al. (2016) Endothelial-specific inhibition of nf-kappab enhances functional haematopoiesis. Nat Commun 7:13829 [PubMed: 28000664]
50. Guo P, Poulos MG, Palikuqi B, Badwe CR, Lis R, Kunar B, Ding BS, Rabbany SY, Shido K, Butler JM et al. (2017) Endothelial jagged-2 sustains hematopoietic stem and progenitor reconstitution after myelosuppression. J Clin Invest 127(12):4242–4256 [PubMed: 29058691]
51. Poulos MG, Guo P, Kofler NM, Pinho S, Gutkin MC, Tikhonova A, Aifantis I, Frenette PS, Kitajewski J, Rafii S et al. (2013) Endothelial jagged-1 is necessary for homeostatic and regenerative hematopoiesis. Cell Rep 4(5):1022–1034 [PubMed: 24012753]
52. Del Gaudio F, Liu D, Lendahl U (2022) Notch signalling in healthy and diseased vasculature. Open Biol 12(4):220004 [PubMed: 35472289]
53. Yang SS, Yu DY, Du YT, Wang L, Gu L, Zhang YY, Xiao M (2020) Inhibition of delta-like ligand 4 enhances the radiosensitivity and inhibits migration in cervical cancer via the reversion of epithelial-mesenchymal transition. Cancer Cell Int 20:344 [PubMed: 32742191]

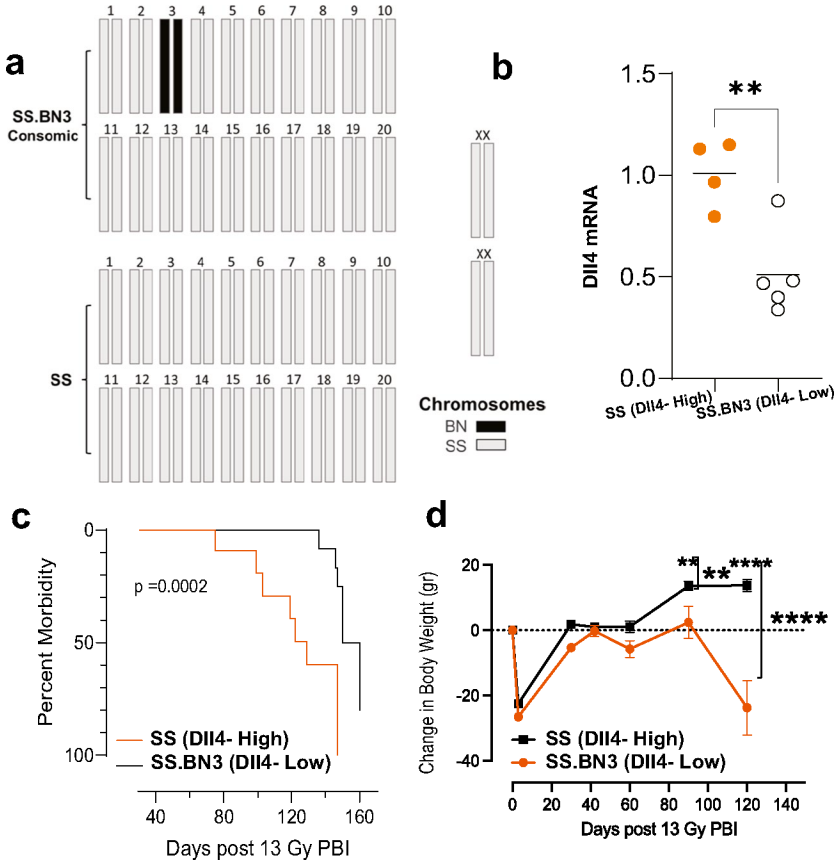

Fig. 1.

SS.BN3 rats have reduced Dll4 expression and reduced susceptibility to late radiation-induced morbidity. **a** Consomic map illustrating the SS.BN3 rat is generated by the substitution of chromosome 3 from the Brown Norway rat into the Dahl-SS genetic background. **b** mRNA expression of Dll4 from $CD31^{+}$ endothelial cells in non-irradiated SS (Dll4-high) and consomic SS.BN3 (Dll4-low) rats ($n = 4$ (SS) or 5 (SS.BN3) rats per group). **c** Survival following 13 Gy partial body irradiation (PBI) in adult SS ($n = 13$) and SS.BN3 rats ($n = 19$). P value for log-rank analysis: $P = 0.0002$ for SS vs SS.BN3 following 13 Gy PBI. **d** Change in body weight relative to pre-irradiation body weight for the rats represented in the survival curve (**$P = 0.0066$, ****$P < 0.0001$, two-way ANOVA Sidak's multiple testing correction). Note the increased drop in body weight at 90 and 120 days in SS as compared to SS.BN3 rats, that occurs during pneumonitis and nephropathy, respectively

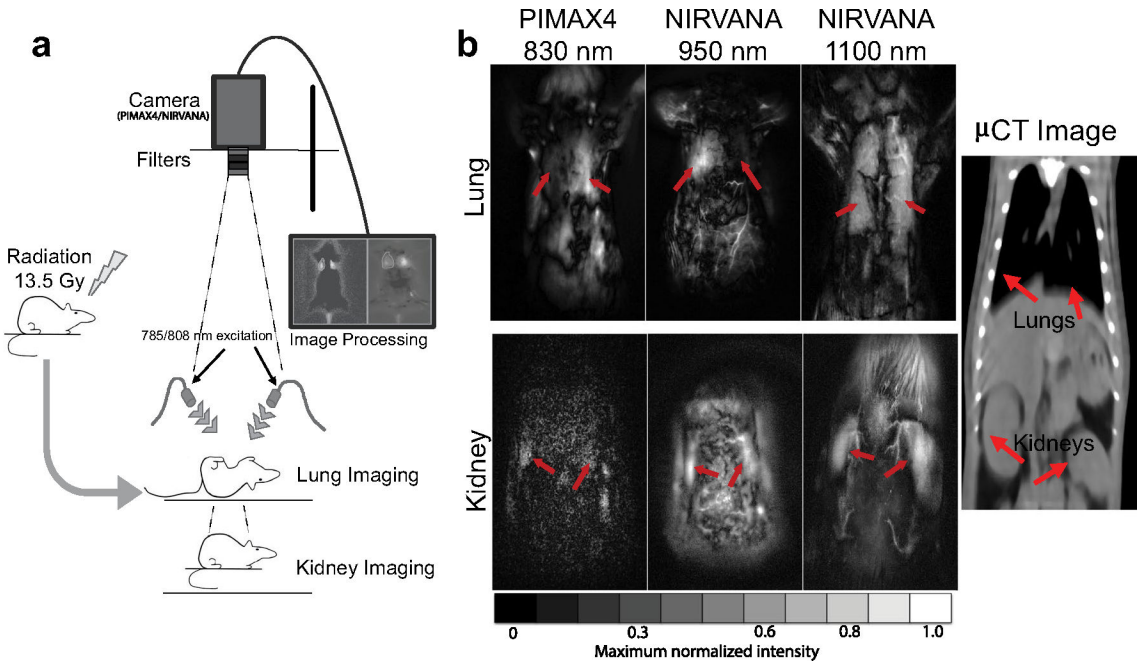

Fig. 2.

Imaging setup and image processing technique. **a** NIR Fluorescence imaging setup using Indocyanine Green optical imaging for the lung and kidney 42 and 90 days after PBI. **b** Determination of region of interest (ROI) for the lung and kidney using principal component analysis (PCA) for 3 different camera setups. Reference lung and kidney locations have been illustrated by using a cross-sectional CT image of a representative SS rat via the SmART 225 kV ortho-voltage x-ray system (Precision X-Ray, North Branford, Connecticut) at 40 kV and 5 mA with 0.2 mm voxels. Time-dependent fluorescence intensity data at each pixel was decomposed into principal components along the time-dimension. The principal components identified to represent lungs and kidneys are illustrated for ICG fluorescence emission windows of 830 nm bandpass, 950 nm long pass, and 1100 nm long pass

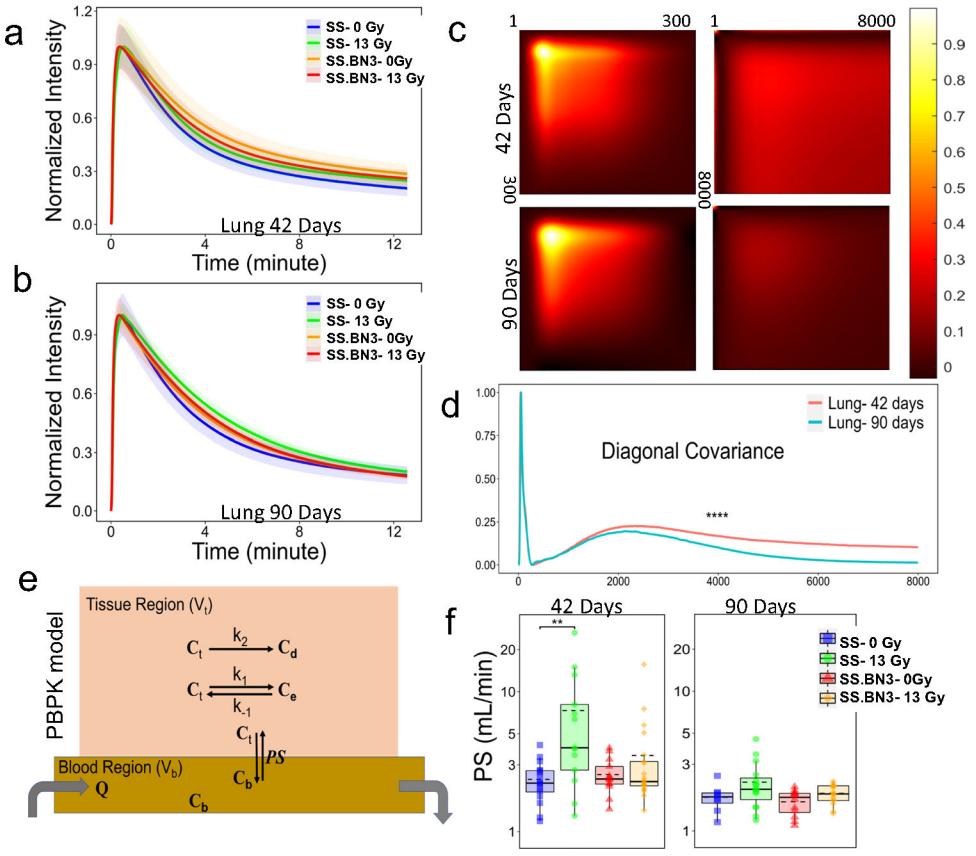

Fig. 3.

SS.BN3 (Dll4-low) rats are protected from radiation-induced increases in lung vascular permeability. **a** Kinetics of ICG uptake and clearance in the right lung at 42 days (a total of 32 SS and 35 SS.BN3 rats, i.e., SS 0 Gy (n = 17), SS 13 Gy (n = 15), SS.BN3 0 Gy (n = 13), and SS.BN3 13 Gy (n = 22)) (solid lines are the average intensity for each group and ribbons represent standard error). **b** ICG fluorescence kinetics of right lung at 90 days following PBI (a total of 22 SS and 29 SS.BN3 rats, i.e., SS 0 Gy (n = 9), SS 13 Gy (n = 13), SS.BN3 0 Gy (n = 12), and SS.BN3 13 Gy (n = 17)) (solid lines are the average intensity for each group and ribbons represent standard error). **c** The mixed-effects covariance model for 8192 and 300 (cropped) timesteps with appropriate time-varying covariates, used to analyze the average fluorescence intensity of ICG in the right lung where subject numbers serve as the repeated measure indicator and the rat strain serving as covariate. **d** The diagonal projection of covariance on a time axis. **e** Physiology-based pharmacokinetic modeling (PBPK) of NIR fluorescence-derived ICG uptake and clearance (ref. 18). The model involves two regions (vascular and tissue regions) and describes the ICG exchange and retention and is used to estimate parameters that significantly affect the ICG uptake by lung, including the permeability of the pulmonary vascular endothelium. **f** The PS (permeability-surface area) product in the right lung at 42 days and 90 days (representing in the **a** and **b**) post PBI (solid and dashed lines represent median and mean respectively)

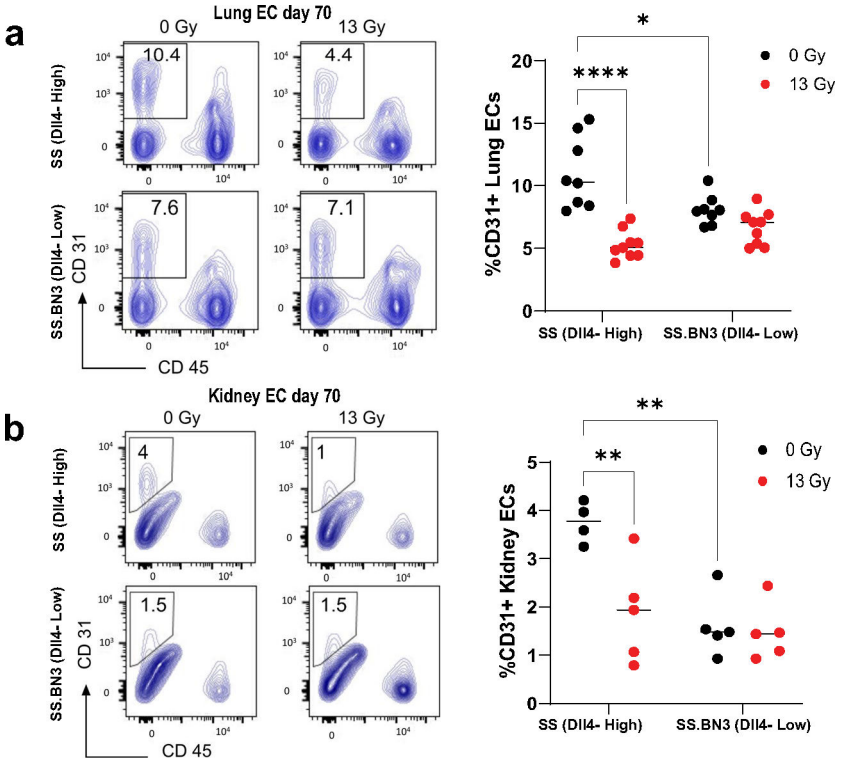

Fig. 4.

SS.BN3 (Dll4-low) rats have reduced radiation-induced loss of $CD31^+$ endothelial cells. **a** Left, representative FACS contour plots showing the percentage of $CD45^-CD31^+$ lung ECs at day 70 following 13 Gy partial body irradiation in SS (Dll4-high) and SS.BN3 (Dll4-low) rats. Right, quantification of percent $CD45^-CD31^+$ cells ($n = 9$ rats per group). **b** Left, representative FACS contour plots showing the percentage of $CD45^-CD31^+$ kidney ECs at day 70 following 13 Gy partial body irradiation in SS (Dll4-high, $n = 4$) and SS.BN3 (Dll4-low, $n = 5$) rats. Right, quantification of percent $CD45^-CD31^+$ cells

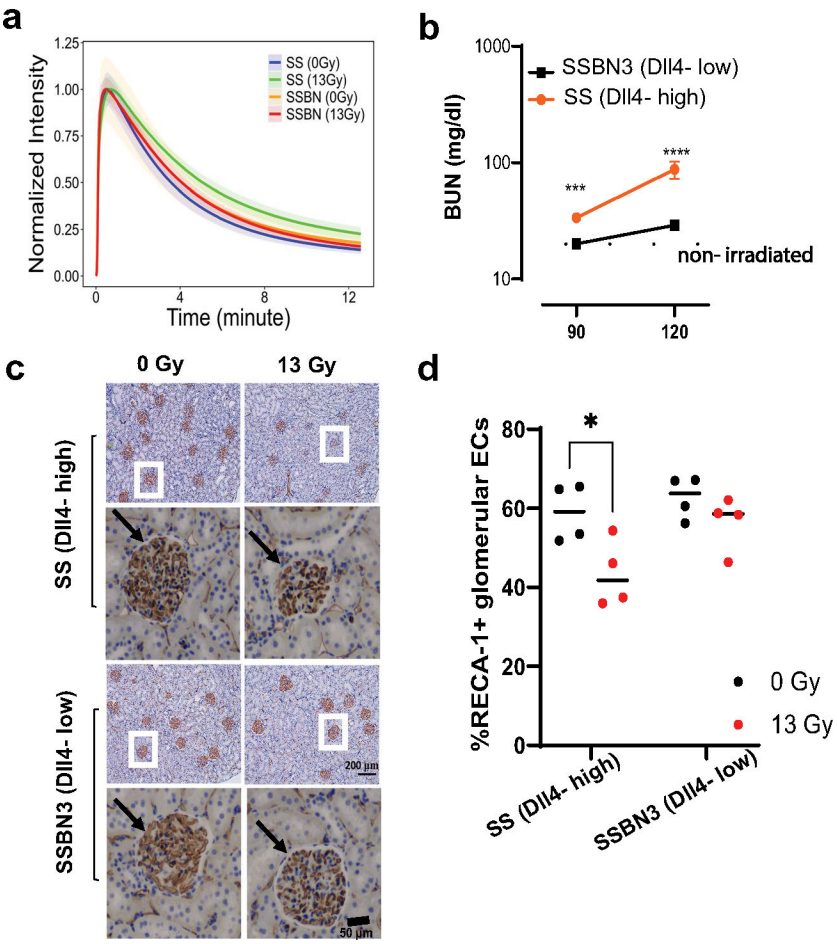

Fig. 5.

SS.BN3 (Dll4-low) are less sensitive to radiation-induced renal vascular damage. **a** ICG fluorescence kinetics in the right kidney at 90 after PBI (a total of 16 SS and 19 SS.BN3 rats, i.e., SS 0 Gy ($n = 11$), SS 13 Gy ($n = 15$), SS.BN3 0 Gy ($n = 7$), and SS.BN3 13 Gy ($n = 12$)) (**$P < 0.01$, two-way ANOVA Sidak's multiple testing correction; solid lines are the average intensity for each group and ribbons represent standard error). **b** Blood urea nitrogen (BUN) levels at days 90 and 120 following 13 Gy PBI in SS (Dll4-high; $n = 30$ for 90 days and $n = 8$ for 120 days) and SS.BN3 (Dll4-low; $n = 37$ for 90 days and $n = 24$ for 120 days) rats. The dashed line depicts mean BUN measurement for all non-irradiated rats ($n = 58$). **c** RECA-1 staining (brown) of renal cortex region, showing the glomeruli at day 70 following 13 Gy PBI in SS and SS.BN3 rats ($n = 4$ for each group). One glomerulus outlined in white from each group is shown in higher magnification (40x) below. **d** Quantification of RECA-1 staining in each group

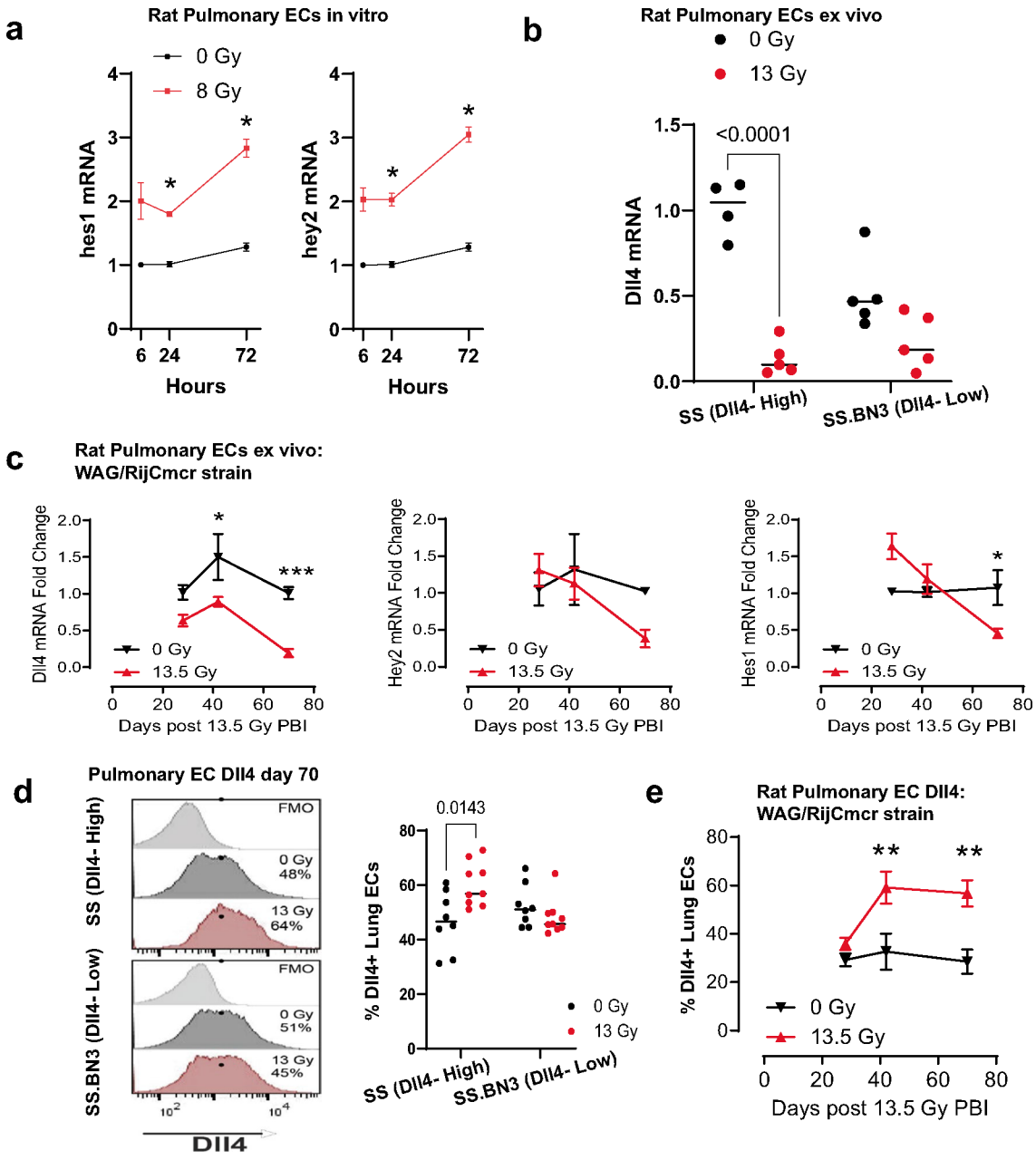

Fig. 6.

Radiation dynamically regulates pulmonary endothelial Dll4 expression. **a** *In Vitro* transcriptional analysis of Notch target genes hes1 and hey2 following *ex vivo* irradiation of rat pulmonary endothelial cells with 8 Gy (n = 3/group). **b** *Ex vivo* transcriptional regulation of Dll4 in pulmonary ECs from SS (Dll4-high) and SS.BN3 (Dll4-low) rats at day 70 following 13 Gy PBI (n = 4 for SS 0 Gy, n = 5 for SS 13 Gy, n = 4 for SS.BN3 0 Gy, and n = 5 for SS.BN3 13 Gy). **c** *Ex vivo* transcriptional regulation of Dll4 and Notch target genes hes1 and hey2 in pulmonary ECs from WagRij/Cmcr at days 28, 42, and 70 following 13.5 Gy PBI (n = 6/group each time point). **d** FACS expression of Dll4 within pulmonary ECs from SS (Dll4-high) and SS.BN3 (Dll4-low) rats at day 70 following 13 Gy (n = 8 for

SS 0 Gy, $n = 9$ for SS 13 Gy, $n = 8$ for SS.BN3 0 Gy, and $n = 9$ for SS.BN3 13 Gy). **e** FACS expression of Dll4 within pulmonary ECs from WagRij/Cmcr at days 28, 42, and 70 following 13.5 Gy ($n = 6$/group each time point)

Table 1

Study design and number of animals for each experiment

Study title		Rat strain (radiation dose)—*n*					
		SS (0 Gy)	SS (13 Gy)	SS.BN3 (0 Gy)	SS.BN3 (13 Gy)	Wag (0 Gy)	Wag (13.5 Gy)
In vivo experiments	Dynamic NIR imaging						
	Lung—42 days	17	15	13	22	-	-
	Lung—90 days	9	13	12	17	-	-
	Kidney—90 days	11	15	7	12	-	-
	Radiation survival study	-	13	-	19	-	-
	Ultra-short echo (UTE) DCE-MRI	4	5	4	5	-	-
Ex vivo experiments	Dll4 transcriptional regulation studies						
	Dll4 expression in pulmonary ECs	4	5	4	5	-	-
	Notch target Hes1 & Hey2 expression (Wag strain), 3 time points	-	-	-	-	6	6
	Vascular protein expression studies						
	FACS $CD45^{-}CD31^{+}$ pulmonary EC counts	9	9	9	9		
	FACS $CD45^{-}CD31^{+}$ renal EC counts	4	4	5	5	-	-
	FACS $Dll4^{+}$ pulmonary EC counts	8	9	8	9	-	-
	FACS $Dll4^{+}$ pulmonary EC counts (Wag strain). 3 time points	-	-	-	-	6	6
	Kidney glomerular ECs RECA-1 immunostaining	4	4	4	4	-	-
	Renal function blood urine nitrogen (BUN) measurements						
	90 days	19	30	20	37	-	-
	120 days	7	8	12	24	-	-